Plasma Chemistry and Gas Conversion

Edited by Nikolay Britun

Modeling for a Better Understanding of Plasma-Based CO$_2$ Conversion

Annemie Bogaerts, Ramses Snoeckx, Georgi Trenchev and Weizong Wang

Abstract

This chapter discusses modeling efforts for plasma-based CO$_2$ conversion, which are needed to obtain better insight in the underlying mechanisms, in order to improve this application. We will discuss two types of (complementary) modeling efforts that are most relevant, that is, (i) modeling of the detailed plasma chemistry by zero-dimensional (0D) chemical kinetic models and (ii) modeling of reactor design, by 2D or 3D fluid dynamics models. By showing some characteristic calculation results of both models, for CO$_2$ splitting and in combination with a H-source, and for packed bed DBD and gliding arc plasma, we can illustrate the type of information they can provide.

Keywords: CO$_2$, plasma chemistry, plasma reactor, fluid dynamics modeling, chemical kinetic modeling

1. Introduction

In recent years, there is increasing interest in plasma-based CO$_2$ conversion [1]. Several types of plasma reactors are being investigated for this purpose, including (packed bed) dielectric barrier discharges (DBDs) [2–10], microwave (MW) plasmas [11–13], and ns-pulsed [14], spark [15], and gliding arc (GA) [16–20] discharges. Research focuses on pure CO$_2$ splitting into CO and O$_2$, as well as on mixtures of CO$_2$ with a hydrogen source, such as CH$_4$ but also H$_2$O or H$_2$, to produce value-added chemicals like syngas, hydrocarbons, and oxygenated products. Key performance indicators are the conversion and the energy efficiency of the process, as well as selectivity to produce specific value-added chemicals. To realize the latter, the plasma should be combined with a catalyst (e.g., [3–5, 21]), as the plasma itself is a too reactive environment and thus not selective.

To improve the application, a good insight in the underlying mechanisms is crucial. This can be obtained by experiments, but modeling the plasma chemistry and reactor design can be a valuable alternative, as it provides information on the most important chemical reaction pathways and on how the geometry and operating conditions can be optimized to improve the results.

In this chapter, we will describe the basics of both plasma chemistry modeling (typically based on 0D chemical kinetic models) and plasma reactor modeling

(typically based on 2D, or even 3D, fluid models), and we will show some characteristic examples from our own research, to illustrate how such models can give more insight in the underlying mechanisms. First, however, we will present a brief overview of the different models relevant to CO_2 conversion that have been reported in literature.

2. Literature overview on modeling for plasma-based CO_2 conversion

Describing a detailed plasma chemistry in 2D or 3D models, with 100s of species and chemical reactions, is not yet feasible, due to excessive calculation times. Therefore, a detailed plasma chemistry is typically described by 0D chemical kinetic models or sometimes by 1D fluid models. The first papers on CO_2 plasma chemistry modeling were published back in 1987–1995 but were applied to CO_2 lasers [22–24]. Some papers also studied the vibrational kinetics of CO_2 for gas flow applications [25, 26]. Rusanov et al. [27] were the first to develop a model for CO_2 conversion in a MW plasma, based on particle and energy conservation equations for the neutral species, and an analytical description of the vibrational distribution function.

In the last decade, the research on plasma-based CO_2 conversion experienced a clear revival, and quite some plasma chemistry models have been developed in literature, for either pure CO_2 splitting [7, 28–48] or CH_4 (of interest for hydrocarbon reforming) [49–52], as well as in various mixtures, that is, CO_2/CH_4 [53–66], CH_4/O_2 [66–72], CO_2/H_2O [73], and CO_2/H_2 [74, 75], of interest for producing value-added chemicals, or in mixtures of CO_2/N_2 [76, 77] or CH_4/N_2 [78–83], more closely mimicking reality, as N_2 is a major component in effluent gases. Recently, we gave an overview of such 0D models for plasma-based CO_2 and CH_4 conversion [84], and we also presented a very comprehensive plasma chemistry model for CO_2 and CH_4 conversion in mixtures with N_2, O_2, and H_2O [85]. These plasma chemistry models can provide detailed information on the underlying chemical reaction pathways for the conversion or product formation.

Furthermore, to investigate which reactor designs can lead to improved CO_2 conversion, 2D or even 3D fluid models can be used; they offer a good compromise between level of detail and calculation time. To our knowledge, the number of 2D models for describing CO_2 conversion is very limited [86, 87], and there exist no 3D models yet for this purpose. Most of the 2D/3D fluid models developed up to now in the literature for the typical plasma reactors used for CO_2 conversion are developed in argon or helium, or sometimes air, with limited chemistry, to reduce the calculation time.

For packed bed DBD reactors, different types of modeling approaches have been developed. Chang [88] presented a 0D plasma chemistry model, simply predicting the enhancement factor of the electric field in the voids between the packing pellets from the ratio of the dielectric constant of the pellets and the gas phase. Takaki et al. [89] applied a simplified time-averaged 1D model in N_2, based on solving the transport equations and Poisson's equation. Zhang et al. [90] performed 2D particle-in-cell/Monte Carlo collision (PIC/MCC) simulations for the filamentary discharge behavior in a parallel-plate packed bed DBD reactor in air. Kang et al. [91] developed a 2D fluid model for a DBD with two stacked ferroelectric beads and studied the propagation of the microdischarges, but no plasma species were explicitly considered. Russ et al. [92] applied a 2D fluid model for studying transient microdischarges in a packed bed DBD operating in dry exhaust gas. Based on a 2D fluid model for a packed bed reactor with dielectric rods, Kruszelnicki et al. [93] presented a very interesting and detailed study on the mechanism of discharge

propagation in humid air, reporting that the discharges can generally be classified in three modalities: positive restrikes, filamentary microdischarges, and surface ionization waves. They observed that the type of discharge dominating the production of reactive species depends on the dielectric facilitated electric field enhancement, which is determined by the topography and orientation of the dielectric lattice. Finally, they demonstrated that photoionization plays an important role in discharge propagation through the dielectric lattice, because it seeds initial charge in regions of high electric field, which are difficult to access for electrons from the main streamer [93]. Van Laer et al. [94–96] developed two complementary 2D fluid models to describe a packed bed DBD in helium, to elucidate the electric field enhancement between the packing beads, and the effect of the dielectric constant of the packing beads, as well as the gap size and bead size. Wang et al. [97] applied a 2D fluid model to a packed bed DBD in air, studying the behavior of positive restrikes, filamentary microdischarges, and surface discharges, as well as the transition in discharge modes upon changing the dielectric constant of the packing beads. Finally, Kang et al. [98] also presented a 2D fluid model to study surface streamer propagation in a simplified packed bed reactor, in comparison with experimental data, obtained from time-resolved ICCD imaging.

For MW plasmas, a large number of models were presented in the literature, and we refer to [99] for a recent overview. Van der Mullen et al. [100–102] as well as Graves et al. [103] developed self-consistent 2D fluid models, based on Maxwell's equations for the electromagnetic field and plasma fluid equations, assuming ambipolar diffusion. Some of these models were applied to intermediate pressure coaxial microwave discharges [102], while others describe atmospheric pressure cylindrical (surfaguide or surfatron) MW plasmas [101, 103]. Although being very valuable, these models did not apply to the application of CO_2 conversion. Recently, Georgieva et al. [99] performed a comparison between two fluid models, based on the coupled solution of the species conservation equations and Poisson's equation (i.e., so-called non-quasi-neutral approach) on the one hand and on a quasi-neutral approach on the other hand, but again these models were developed for argon.

For low-current nonthermal GA discharges (typically near 1 A or below), some simple 1D analytical or semi-analytical models have been developed [104–109], including the plasma string model [104] and the Elenbaas-Heller model, assuming an equilibrium plasma, with the radius of the plasma channel being constant [105–107] or with a correction based on an analytical relation between the electric field and the electron and gas temperatures for non-equilibrium plasma [108] or focusing on the discharge electrical parameters [109]. These simple models cannot describe the complex behavior of the GA, such as the unsteady behavior in time and space, arc restrike, non-equilibrium effects, effects of flow patterns, etc., and they did not include a detailed chemistry. Gutsol and Gangoli [110] presented a simple 2D model of a GA, in a plane parallel to the gas flow and perpendicular to the discharge current, which provided very useful information about the gas-discharge interaction. Within our group, we developed a 2D non-quasi-neutral fluid model for the arc gliding process in an argon GA [111], and we compared the glow and arc mode in this setup [112]. We also presented a 2D quasi-neutral model [113], which was also applied in 3D modeling for a classical (diverging electrode) GA [114] and a reverse vortex flow (RVF) GA (also called GA plasmatron; GAP) [115]. These models were developed for argon, but we also developed a 1D fluid model [44] and two different 2D models [86, 87] for a (classical or RVF) GA in CO_2, considering the detailed plasma chemistry of CO_2 conversion. An overview of both 0D chemical kinetic models and 2D/3D fluid models for plasma reactors of interest for CO_2 conversion was presented in [116].

3. Explanation of the modeling approaches

3.1 0D chemical kinetic modeling

Most models describing a detailed plasma chemistry apply the 0D chemical kinetic approach, which allows to handle a large number of species and chemical reactions, with limited computational effort. This approach is based on solving balance equations for the various species densities, based on production and loss rates, as defined by chemical reactions:

$$\frac{dn_i}{dt} = \sum_j \left\{ \left(a_{ij}^{(2)} - a_{ij}^{(1)} \right) k_j \prod_l n_l^{a_{lj}^{(1)}} \right\} \qquad (1)$$

where $a_{ij}^{(1)}$ and $a_{ij}^{(2)}$ are the stoichiometric coefficients of species i, at the left- and right-hand sides of a reaction j, respectively, n_l is the species density at the left-hand side of the reaction, and k_j is the rate coefficient of reaction j. For the electron reactions, the energy-dependent rate coefficients are determined from the average electron energy, while the rate coefficients of the chemical reactions between neutral species or ions are adopted from the literature.

The species typically included in such models, for either pure CO_2 or pure CH_4, as well as the extra species included in CO_2/CH_4, CO_2/H_2O, CO_2/H_2, or CH_4/O_2 gas mixtures and in CO_2/N_2 and CH_4/N_2 mixtures are listed in **Table 1**. The same species can be included in the CO_2/CH_4, CO_2/H_2O, CO_2/H_2, and CH_4/O_2 models, because these combinations produce similar molecules. All the species listed in **Table 1** might chemically react with each other. Hence, a large number of chemical reactions (typically up to 1000) are incorporated in these models, including electron impact reactions, electron-ion recombination, and ion-ion, ion-neutral, and neutral-neutral reactions. Details of these chemistries for the specific gas mixtures can be found, for example, in [7, 28–30, 61–63, 66, 73–77, 83].

Specifically for CO_2 conversion in MW and GA plasmas, the vibrational levels of CO_2 are very important, because they allow energy-efficient CO_2 conversion [117], so the vibrational kinetics of CO_2 must be incorporated and especially the asymmetric stretch mode of CO_2, which is the most important channel for dissociation [117]. Likewise, in CO_2/N_2 mixtures in MW or GA discharges, the N_2 vibrational levels must be included, as they can populate the CO_2 vibrational levels [76]. Furthermore, also the vibrational levels of CO and O_2, and some electronically excited levels, are typically taken into account in such models (see **Table 1**). These vibrationally and electronically excited levels are indicated in **Table 1** with the symbols "V" and "E". Details about their notations can be found in [29, 76] or in **Table 1** for the N_2 electronically excited levels. Although vibrationally excited levels might also be important for CH_4, H_2O, and H_2 molecules, they are not yet included in the available models, to our knowledge, as these mixtures have only been described up to now for a DBD plasma, where the vibrational levels are of minor importance [117].

Although the above balance equations only account for time variations, thus neglecting spatial variations due to transport in the plasma, spatial variations can be included in such models, by imposing a certain input power or gas temperature as a function of time. For instance, this allows to account for microdischarge filaments in a DBD, through which the gas molecules pass when flowing through the reactor, by applying a number of pulses as a function of time (see, e.g., [28, 48, 62]). In a similar way, this method can account for the power deposition profile in a MW plasma (being at maximum at the position of the waveguide) by means of a temporal profile. Thus, the plasma reactors are considered as plug flow reactors, where

Molecules	Charged species	Radicals	Excited species
Species of interest in pure CO$_2$ models			
CO_2, CO	CO_2^+, CO_4^+, CO^+, $C_2O_2^+$, $C_2O_3^+$, $C_2O_4^+$, C_2^+, C^+, CO_3^-, CO_4^-	C_2O, C, C_2	$CO_2(V_a, V_b, V_c, V_d)$, $CO_2(V1-V21)$, $CO_2(E1, E2)$, $CO(V1-V10)$, $CO(E1-E4)$
O_2, O_3	O^+, O_2^+, O_4^+, O^-, O_2^-, O_3^-, O_4^-	O	$O_2(V1-V4)$, $O_2(E1-E2)$
	Electrons		
Species of interest in pure CH$_4$ models			
CH_4	CH_5^+, CH_4^+, CH_3^+, CH_2^+, CH^+, C^+	CH_3, CH_2, CH, C	CH_4^*
C_2H_6, C_2H_4, C_2H_2, C_2	$C_2H_6^+$, $C_2H_5^+$, $C_2H_4^+$, $C_2H_3^+$, $C_2H_2^+$, C_2H^+, C_2^+	C_2H_5, C_2H_3, C_2H	$C_2H_6^*$, $C_2H_4^*$, $C_2H_2^*$
C_3H_8, C_3H_6, C_4H_2		C_3H_7, C_3H_5	$C_3H_8^*$
H_2	H_3^+, H_2^+, H^+, H^-	H	H_2^*
Extra species typically included in CO$_2$/CH$_4$, CO$_2$/H$_2$O, CO$_2$/H$_2$ or CH$_4$/O$_2$ models			
H_2O, H_2O_2	H_3O^+, H_2O^+, OH^+, OH^-	OH, HO_2	H_2O^*
CH_2O, CH_3OH, CH_3OOH		CHO, CH_2OH, CH_3O, CH_3O_2	
C_2H_5OH, C_2H_5OOH, CH_3CHO, CH_2CO		$CHCO$, CH_3CO, CH_2CHO, C_2H_5O, $C_2H_5O_2$	
Extra species typically included in CO$_2$/N$_2$ and/or CH$_4$/N$_2$ models			
N_2	N^+, N_2^+, N_3^+, N_4^+	N	$N_2(V1-V14)$, $N_2(C^3\Pi_u)$, $N_2(A^3\Sigma_u^+)$, $N_2(a'^1\Sigma_u^-)$, $N_2(B^3\Pi_g)$, $N(2D)$, $N(2P)$
N_2O, N_2O_3, N_2O_4, N_2O_5	NO^+, N_2O^+, NO_2^+, NO^-, N_2O^-, NO_2^-, NO_3^-, $N_2O_2^+$	NO, NO_2, NO_3	
HCN, $ONCN$, C_2N_2	HCN^+	H_2CN, CN, NCO, NCN	
NH_3	NH_4^+, NH_3^+, NH_2^+, NH^+	NH_2, NH	NH_3^*
N_2H_4, N_2H_2		N_2H_3, N_2H	

Table 1.
Overview of the species typically included in plasma chemistry models for pure CO$_2$, pure CH$_4$, as well as extra species included in CO$_2$/CH$_4$, CO$_2$/H$_2$O, CO$_2$/H$_2$, and CH$_4$/O$_2$ gas mixtures and in CO$_2$/N$_2$ or CH$_4$/N$_2$ mixtures.

the plasma characteristics vary as a function of distance traveled by the gas, in the same way as they would vary in time in a batch reactor. The time in the balance equations thus corresponds to a residence time of the gas in the reactor, and the time variation can be translated into a spatial variation by means of the gas flow rate.

Besides balance equations for the species densities, 0D chemical kinetic models typically also apply balance equations for the electron temperature and/or the gas temperature, again based on source and loss terms, defined by the power deposition (or electric field) and the chemical reactions. Alternatively, instead of calculating the electron temperature with a balance equation, 0D models often solve a Boltzmann equation (e.g., Bolsig+ [118]), to calculate the electron energy distribution function (EEDF) and the rate coefficients of the electron impact reactions as a

function of the electron energy. A more detailed description of the free electron kinetics in CO_2 plasma is provided in [32–37], where a state-to-state vibrational kinetic model was self-consistently coupled with the time-dependent electron Boltzmann equation.

0D models allow to predict the gas conversion, the product yields, and selectivities, based on the calculated plasma species densities at the beginning and the end of the simulations, corresponding to the inlet and outlet of the plasma reactor. Furthermore, based on the power introduced in the plasma and the gas flow rate, the specific energy input (SEI) can be computed, and from the latter, the energy efficiency (η) can be obtained with the following formulas:

$$SEI\left(\frac{kJ}{l}\right) = \frac{Plasma\,power(kW)}{Flow\,rate\left(\frac{l}{\min}\right)} * 60\left(\frac{s}{\min}\right) \qquad (2)$$

$$\eta(\%) = \frac{\Delta H_R\left(\frac{kJ}{mol}\right) * X_{CO_2}(\%)}{SEI\left(\frac{kJ}{l}\right) * 22.4\left(\frac{l}{mol}\right)} \qquad (3)$$

where ΔH_R is the reaction enthalpy of the reaction under study (e.g., 279.8 kJ/mol for CO_2 splitting) and X_{CO_2} is the CO_2 conversion. Note that this formula is only applicable to pure CO_2 splitting, but a similar formula can be applied to the other gas mixtures, using another reaction enthalpy and accounting not only for the CO_2 conversion but also for the conversion of the other gases in the mixture.

3.2 2D or 3D fluid modeling

Even though some spatial dependences of the plasma reactors can be taken into account in 0D chemical kinetic models, as explained above, they are not really suitable for describing detailed plasma reactor configuration or predict how modifications to the reactor geometry would give rise to better CO_2 conversion and energy efficiency. For this purpose, 2D or even 3D models are required, and fluid models are then the most logical choice, because they still allow a reasonable calculation time, in contrast to, for instance, PIC-MCC simulations.

These fluid models solve a number of conservation equations for the densities of the various plasma species and for the average electron energy. The energy of the other plasma species can be assumed in thermal equilibrium with the gas. The conservation equations for the species densities are again based on source and loss terms, defined by the chemical reactions, like in the 0D models. The source of the electron energy is due to heating by the electric field, and the energy loss is again dictated by collisions. In addition, transport is now included in the conservation equations, defined by diffusion and by migration in the electric field (for the charged species) and (in some cases) by convection due to the gas velocity. Furthermore, the conservation equations are coupled with Poisson's equation for a self-consistent calculation of the electric field distribution from the charged species densities, although more simplified quasi-neutral (QN) models have also been used [113], to further reduce the calculation time. Such a QN model neglects the near-electrode regions and treats only the quasi-neutral bulk plasma. It does not solve the Poisson equation, but calculates the ambipolar electric field from the ion densities and the electron and ion diffusion coefficients and mobilities.

Finally, in many cases, the gas temperature and gas flow behavior are calculated with a heat transfer equation and the Navier-Stokes equations, respectively, while in GA models, the cathode heat balance can also be accounted for, to properly describe the electron emission processes. The fluid (plasma) model and the models

for gas flow and gas heating are typically combined into a multiphysics model: the calculated gas velocity is inserted in the transport equations of the plasma species, and the gas temperature determines the gas density profile and thus the chemical reaction rates.

4. Some typical calculation results

4.1 0D chemical kinetic modeling

0D chemical kinetic models typically provide information about the calculated gas conversion, energy efficiency, and product formation, as a function of specific operating conditions, as well as about the underlying chemistry explaining these results. The latter will be illustrated here, based on the modeling work performed within our group PLASMANT, for pure CO_2 splitting, as well as CO_2/CH_4, CH_4/O_2, CO_2/H_2, and CO_2/H_2O mixtures. For more details about the modeling results in these mixtures, and more specifically the calculated conversions, product yields and energy efficiencies, and comparison with experiments, we refer to the original research papers mentioned below, as well as two recent review papers [84, 116].

#### 4.1.1 Pure CO_2 splitting

4.1.1.1 DBD conditions

The dominant reaction pathways for CO_2 splitting in a DBD plasma, as predicted from the model in [7], are plotted in **Figure 1**. As a DBD is characterized by relatively highly reduced electric field values (typically above 200 Td), and thus relatively high electron energies (several eV), electron impact reactions with CO_2 ground-state molecules dominate the chemistry. The most important reactions are electron impact dissociation into CO and O (which proceeds through electronically excited CO_2, that is, the so-called electron impact excitation-dissociation), electron impact ionization into CO_2^+ (which recombines with electrons or O_2^- ions into CO and O and/or O_2), and electron dissociative attachment into CO and O^- (cf. the thick black arrow lines in **Figure 1**). These three processes account for about 50%, 25%, and 25%, respectively, to the total CO_2 conversion [28]. Because these processes require more energy than strictly needed for breaking the C=O bond (i.e., 5.5 eV), the energy efficiency for CO_2 splitting in a DBD plasma is quite limited, that is, up to maximum 10% for a conversion up to 30% [1].

The CO molecules are relatively stable, but at very long residence time, they will recombine with O^- ions or O atoms, to form again CO_2 (cf. thin black arrow lines in **Figure 1**). This explains why the CO_2 conversion typically saturates at long residence times. Furthermore, the O atoms created upon CO_2 splitting also recombine quickly into O_2 or O_3, based on several processes (see also **Figure 1**).

4.1.1.2 MW and GA conditions

While our calculations predict that ca. 94% of the CO_2 splitting in a DBD plasma arises from the ground state, and only ~6% occurs from the vibrationally excited levels [28], the situation is completely different in a MW or GA plasma. These plasmas are characterized by much lower reduced electric field values (in the order of 50–100 Td), creating lower electron energies (order of 1 eV), which are most suitable for vibrational excitation of CO_2. Therefore, the CO_2 splitting in MW and GA discharge is mainly induced by electron impact vibrational excitation of the
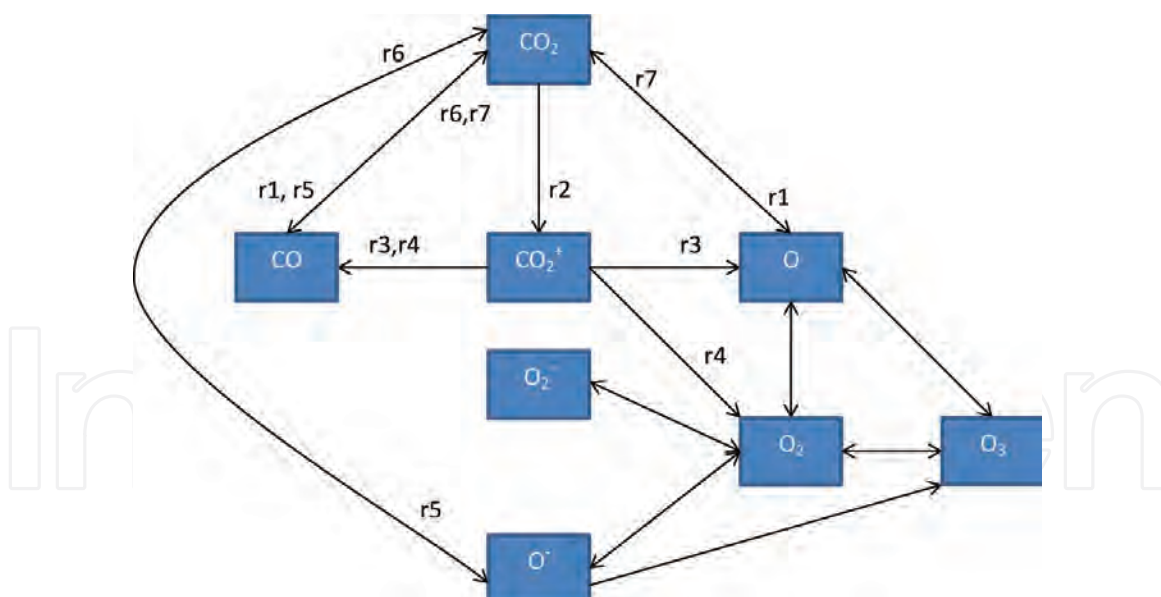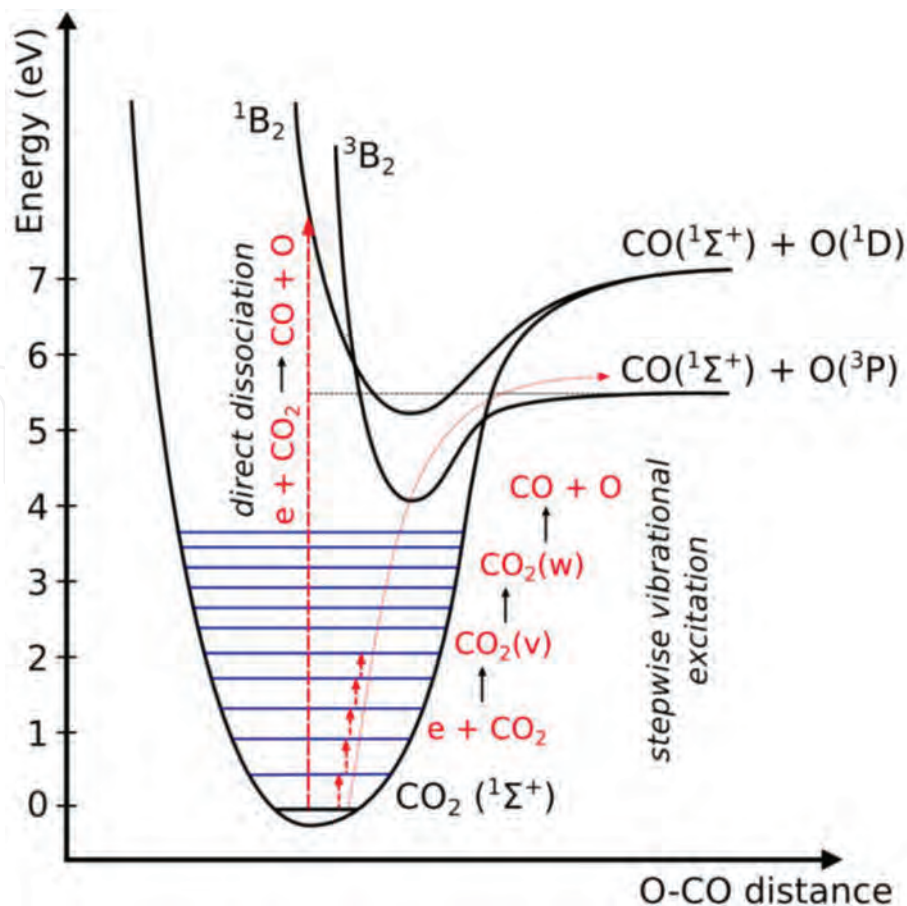
Figure 1.
Dominant reaction pathways of CO_2 splitting and the further reactions between O, O_2, and O_3 in a DBD plasma, as obtained from the model in [7], where the labels are also explained. Adopted from [119] with permission.

lowest vibrational levels, followed by vibrational-vibrational (VV) collisions, gradually populating the higher vibrational levels, leading to dissociation of CO_2. This stepwise vibrational excitation, or the so-called ladder climbing, is illustrated in **Figure 2**. As this process only requires 5.5 eV for dissociation, that is, exactly the C=O bond energy, this explains why MW and GA discharges exhibit a much better energy efficiency than a DBD, where the dominant dissociation mechanism is electron impact excitation-dissociation, as explained above, which requires 7–10 eV (see **Figure 2**).

Still, it must be realized that the vibrational excitation pathway is not always optimized in a MW or GA plasma. Indeed, as illustrated in detail in [42], the vibrational excitation is higher at lower pressures and higher power densities. The latter give rise to higher electron densities, which yield more vibrational excitation. Higher pressures, on the other hand, result in more vibrational-translational (VT) relaxation collisions, which represent the major loss mechanism of the vibrational energy. Finally, also the gas temperature plays a crucial role, as a higher gas temperature also results in more pronounced VT relaxation. Our models predict that in a MW plasma at atmospheric pressure, the dissociation is too much determined by thermal processes, thus limiting the CO_2 conversion and energy efficiency, in agreement with experimental observations. In addition, the recombination of CO and O atoms also becomes gradually more important at high gas temperature and pressures [42], further explaining why the experimental CO_2 conversion and energy efficiency drop upon increasing pressure. The main processes occurring in a MW plasma in the two extreme cases, that is, the ideal non-equilibrium conditions of low pressure and temperature and high power density and the near-thermal conditions of high pressure and temperature, are summarized in **Figure 3**. The model predicts a much higher CO_2 conversion and energy efficiency in a pressure range of 200–300 mbar and much lower values at atmospheric pressure, in the near-thermal conditions [42]. Hence, we should exploit as much as possible the non-equilibrium character of a MW plasma, in which the higher vibrational levels of CO_2 are overpopulated, to obtain the most energy-efficient CO_2 conversion.

The same conclusions can be drawn for a GA plasma, where our models predict that the CO_2 conversion could be further enhanced, by exploiting the role of the
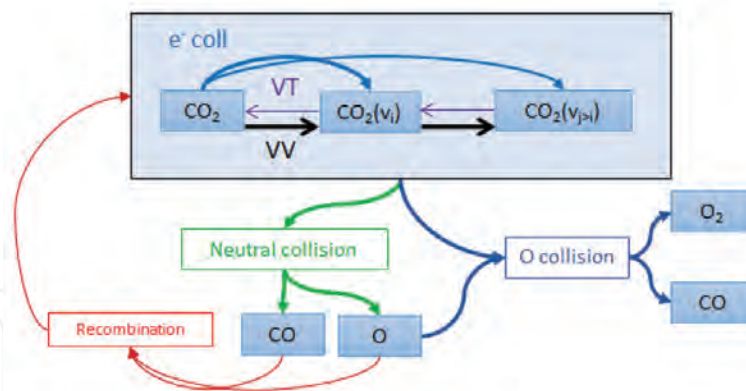
Figure 2.
Schematic illustration of some CO$_2$ electronic and vibrational levels, illustrating the energy-efficient dissociation process through electron impact vibrational excitation, followed by vibrational-vibrational collisions, which gradually populate the higher vibrational levels, that is, the so-called ladder climbing (5.5 eV), compared to direct dissociation through electronic excitation (above 7 eV). Adopted from [119] with permission.

higher vibrational levels of CO$_2$. Indeed, as the GA operates at atmospheric pressure, the vibrational distribution function (VDF) is too much thermal, that is, there is no significant overpopulation of the higher CO$_2$ vibrational levels. This was predicted both in a classical GA at a temperature around 1200 K [45] and in a RVF GA, operating at temperatures around 2500–3000 K [47]. The CO$_2$ dissociation even proceeds mainly from the ground state or the lowest vibrational levels. Indeed, based on these models, the major dissociation process was electron impact dissociation [45] or thermal dissociation [47] of the lower CO$_2$ vibrational levels, and the chemical reactions of the higher vibrational levels (with either O atoms or any arbitrary molecules in the plasma), which theoretically provide the most energy-efficient process for CO$_2$ conversion, were found to be of minor importance. Just like in the MW plasma, the model predicts that a significant overpopulation of the VDF, and thus a more energy-efficient CO$_2$ conversion, can be realized by decreasing the temperature or by increasing the power density [45].

4.1.2 CO$_2$/CH$_4$ mixture

When adding an H-source, such as CH$_4$, to the CO$_2$ plasma, a variety of molecules can be formed, with a mixture of H$_2$ and CO (or syngas) as the major compounds, but also smaller fractions of higher hydrocarbons and oxygenates can be formed. **Figure 4** illustrates the dominant pathways in a CO$_2$/CH$_4$ mixture, as predicted by the model in [66]. The thickness of the arrow lines is correlated to the rate of the reaction. CH$_4$ dissociation is initiated by electron impact, forming CH$_3$
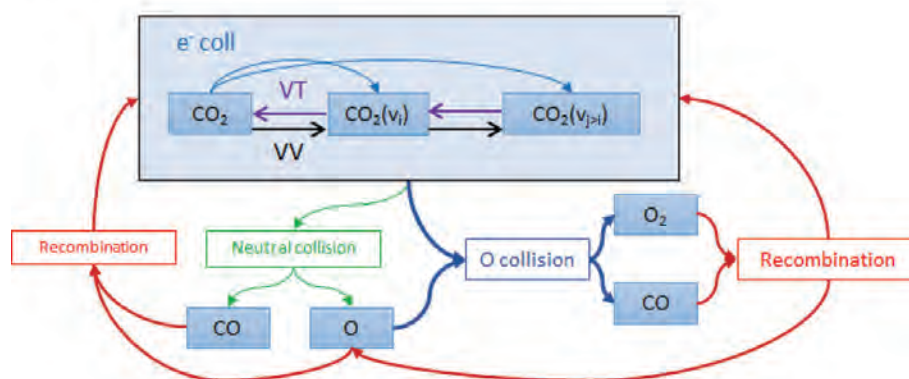
Figure 3.
Dominant reaction pathways of CO_2 splitting in a MW plasma, as obtained from the model in [42], for two extreme cases: (a) the ideal non-equilibrium conditions of low pressure and temperature and high power density and (b) the near-thermal condition of high pressure and temperature. Adopted from [116] with permission.

radicals, which recombine into higher hydrocarbons. Moreover, electron impact dissociation of CH_4 and of the higher hydrocarbons also yields H_2 formation. In addition, the CH_3 radicals also create methanol (CH_3OH) and CH_3O_2 radicals, albeit to a lower extent. Furthermore, the CH_2 radicals, also created from electron impact dissociation of CH_4, react with CO_2 to form formaldehyde (CH_2O) and CO. Finally, the O atoms, created from electron impact dissociation of CO_2 (see also **Figure 1**), also initiate the formation of higher oxygenates, like acetaldehyde (CH_3CHO). This species reacts further into CH_3CO radicals and subsequently into ketene (CH_2CO), although these pathways are not so important in absolute terms, as indicated by the thin dashed lines in **Figure 4**.

We have also compared the chemistry in the CO_2/CH_4 mixture, used for dry reforming of methane, with that of partial oxidation of methane, that is, a CH_4/O_2 mixture [66]. The reaction pathways of the latter are depicted in **Figure 5**. The CH_4/O_2 mixture clearly leads to a completely different chemistry than the CO_2/CH_4
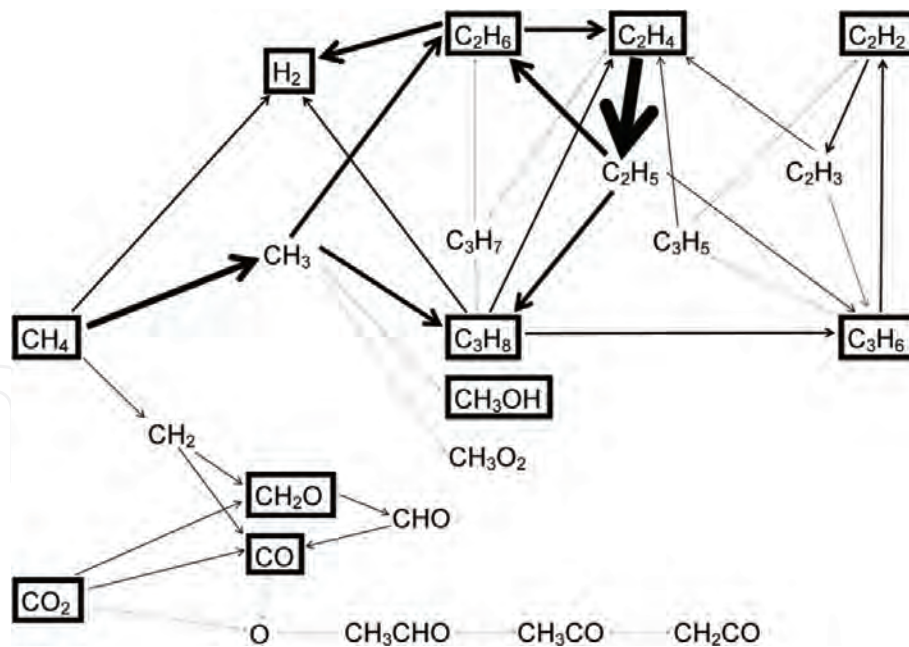
Figure 4.
Dominant reaction pathways for the conversion of CH$_4$ and CO$_2$ into higher hydrocarbons, H$_2$ and CO, and higher oxygenates, in a 70/30 CH$_4$/CO$_2$ DBD plasma, as obtained from the model in [66]. The thickness of the arrow lines corresponds to the importance of the reaction paths. Reproduced from [84] with permission.
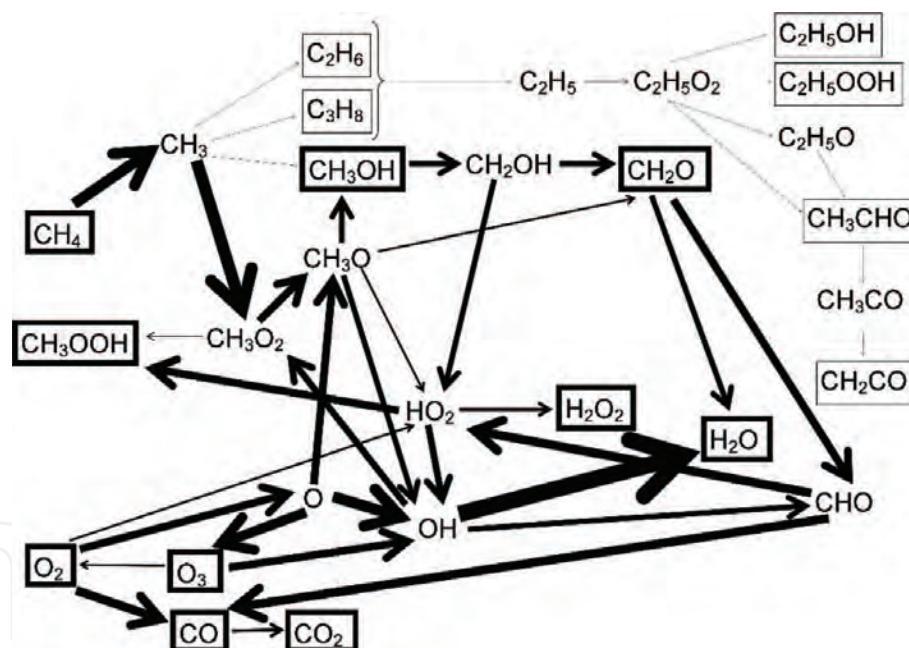
Figure 5.
Dominant reaction pathways for the conversion of CH$_4$ and O$_2$ into (mainly) higher oxygenates, as well as some full oxidation products, in a 70/30 CH$_4$/O$_2$ DBD plasma, as obtained from the model in [66]. The thickness of the arrow lines corresponds to the importance of the reaction paths. Reproduced from [84] with permission.

mixture, in spite of the fact that the same chemical species are included in the models (see **Table 1**). Electron impact dissociation of CH$_4$ again produces CH$_3$ radicals, which will recombine into methanol or higher hydrocarbons, but the recombination into CH$_3$O$_2$ radicals, which form either CH$_3$O radicals or methyl hydroperoxide (CH$_3$OOH), is now more important. The CH$_3$O radicals produce methanol, which seems a more important formation mechanism than the recombination of CH$_3$ with OH radicals (cf. the arrow line thickness in **Figure 5**), and methanol can also react further into CH$_2$OH radicals, producing formaldehyde. The latter is also easily converted into CHO radicals and further into CO (note the

thickness of these arrow lines, indicating the importance of these reactions) and CO_2. Furthermore, formaldehyde is also partially converted into H_2O. Note that this pathway is illustrated for a 70/30 CH_4/O_2 mixture, which obviously leads to nearly full oxidation of CH_4, rather than partial oxidation, where the major end products should be the higher oxygenates. When less O_2 would be present in the mixture, our model predicts that methanol and methyl hydroperoxide are formed in nearly equal amounts as CO and H_2O [66]. **Figure 5** also illustrates that the O_2 molecules are mainly converted into CO, O atoms, and HO_2 radicals. Some O_3 is also formed out of O_2, but the reverse process, that is, the production of two O_2 molecules out of O_3 and O atoms, is more important, explaining why the arrow points from O_3 toward O_2. The O atoms are converted into CH_3O and OH radicals, producing methanol and water, respectively. The latter reaction (from OH to H_2O) appears to be very important (cf. thick arrow line in **Figure 5**), and thus, significant amounts of H_2O are formed, as predicted by the model [66].

In summary, comparing **Figures 4** and **5** clearly indicates that the chemical pathways in CH_4/O_2 and CH_4/CO_2 plasma are quite different, even at the same mixing ratios. Finally, in both mixtures a large number of different chemical compounds can be formed, but due to the reactivity of the plasma, there is no selective production of some targeted compounds. To reach the latter, the plasma will have to be combined with a catalyst.

4.1.3 CO_2/H_2 mixture

The dominant reaction pathways for the conversion of CO_2 and H_2 in a 50/50 CO_2/H_2 DBD plasma are illustrated in **Figure 6**, as predicted by the model in [75]. The conversion starts again with electron impact dissociation of CO_2, yielding CO and O atoms. Simultaneously, electron impact dissociation of H_2 results in the formation of H atoms, and this reaction seems more important (cf. the thickness of the arrow line). The O and H atoms recombine into the formation of OH radicals and further into H_2O. The model thus predicts that H_2O is produced at relatively high density [75]. The CO molecules will partially react back into CO_2, mainly through the formation of CHO radicals. This pathway appears to be more important than the direct three-body recombination between CO and O atoms into CO_2, which is the dominant pathway in a pure CO_2 plasma. The H atoms thus contribute
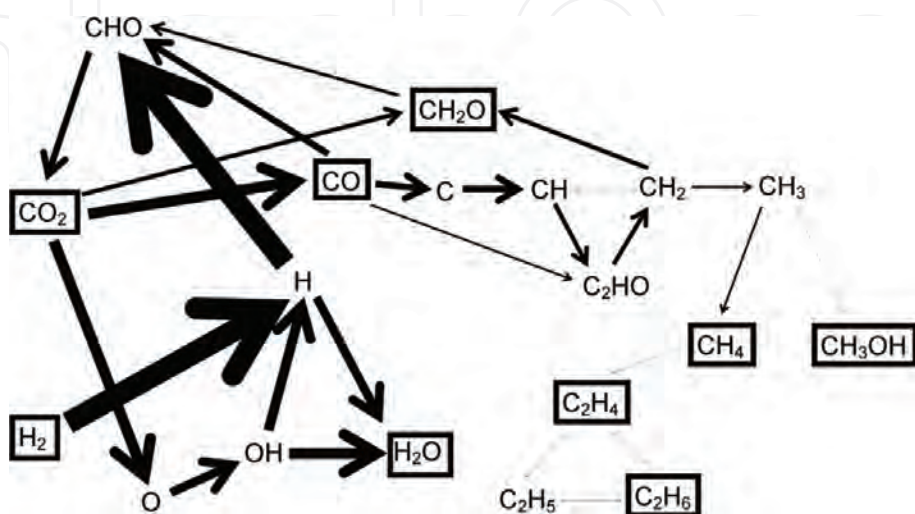
Figure 6.
Dominant reaction pathways for the conversion of CO_2 and H_2 into various products, in a 50/50 CO_2/H_2 DBD plasma, as obtained from the model in [75]. The thickness of the arrow lines corresponds to the rates of the net reactions. The stable molecules are indicated with black rectangles. Reproduced from [75] with permission.
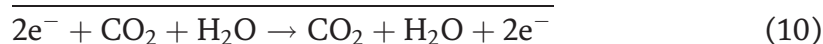
significantly to the back reaction of CO into CO$_2$, and this explains why the calculated CO$_2$ conversion is quite limited in a CO$_2$/H$_2$ mixture [75]. Electron impact dissociation of CO yields the formation of C atoms, which react further into CH, CH$_2$, C$_2$HO, and CH$_3$ radicals in several successive radical recombination reactions. The CH$_2$ radicals react with CO$_2$ into CH$_2$O, while the CH$_3$ radicals easily form CH$_4$. The latter reaction is more favorable than CH$_3$OH formation out of CH$_3$. Finally, CH$_4$ partially reacts further into higher hydrocarbons (C$_x$H$_y$).

Figure 6 clearly illustrates that several subsequent radical reactions are required for the formation of (higher) hydrocarbons and oxygenates. This explains the very low calculated yields and selectivities of these end products [75]. In summary, the lack of direct formation of CH$_2$ and CH$_3$ in the CO$_2$/H$_2$ mixture, which is important in CO$_2$/CH$_4$ gas mixtures (see **Figure 4**), combined with the very low conversion of CO$_2$, which is again attributed to the absence of CH$_2$ as important collision partner for the loss of CO$_2$, makes the CO$_2$/H$_2$ mixture less interesting for the formation of higher hydrocarbons and oxygenates than a CO$_2$/CH$_4$ mixture at the conditions under study. Furthermore, as H$_2$ is a useful product by itself, while CH$_4$ is also a greenhouse gas (besides a fuel), the simultaneous conversion of CO$_2$ and CH$_4$, that is, two greenhouse gases, is considered to be of higher value, also because it represents a direct valorization of biogas.

4.1.4 CO$_2$/H$_2$O mixture

H$_2$O is the cheapest H-source to be added to a CO$_2$ plasma for the direct production of value-added chemicals, and the combined conversion of CO$_2$ and H$_2$O could mimic the natural photosynthesis process. However, adding H$_2$O (in concentrations up to 8%) to a CO$_2$ DBD plasma causes a significant reduction in the CO$_2$ conversion, while no oxygenated hydrocarbons were detected experimentally, and also the calculated concentrations were only in the ppb level [73].

These results can be explained by a kinetic analysis of the reaction chemistry. The latter reveals that the reaction between CO and OH, yielding H atoms and CO$_2$, is crucial, as it has a very high rate constant, and it controls the ratio between the conversions of CO$_2$ and H$_2$O. This can be explained in a very simple way by the following reactions:

$$e^- + CO_2 \rightarrow CO + O + e^- \tag{4}$$

$$e^- + H_2O \rightarrow OH + H + e^- \tag{5}$$

$$CO + OH \rightarrow CO_2 + H \tag{6}$$

$$H + O_2 + M \rightarrow HO_2 + M \tag{7}$$

$$HO_2 + O \rightarrow OH + O_2 \tag{8}$$

$$OH + H \rightarrow H_2O \tag{9}$$

$$\overline{2e^- + CO_2 + H_2O \rightarrow CO_2 + H_2O + 2e^-} \tag{10}$$

Reactions (4) and (5) yield the dissociation of CO$_2$ and H$_2$O, but the products, CO and OH, will rapidly recombine into CO$_2$ again (reaction (6)). Moreover, the two H atoms and one O atom formed will also quickly recombine, first into OH (through subsequent reactions (7) and (8)) and subsequently into H$_2$O through reaction (9). Thus, overall, there is no net dissociation of CO$_2$ and H$_2$O in this pathway (see overall reaction (10)).

Of course, there exist also other pathways for the conversion of these molecules, so there will still be some conversion of CO$_2$ and H$_2$O in the plasma, but electron

impact dissociation is typically the major loss mechanism for CO_2 in a DBD (cf. also above), so the above mechanism explains the drop in CO_2 conversion upon addition of H_2O, as the OH radicals created upon H_2O dissociation give rise to the back reaction, creating CO_2 out of CO.

The above mechanism can also explain why no (significant) methanol (or other oxygenated hydrocarbons) is formed in the CO_2/H_2O mixture, because all the H atoms needed to form CH and CHO fragments for the formation of methanol are steered to OH and subsequently H_2O again. Hence, this chemical kinetic analysis indicates that H_2O might not be a suitable H-source for the formation of oxygenated hydrocarbons in a one-step process, because of the abundance of O atoms, O_2 molecules, and OH radicals, trapping the H atoms.

It should be noted that this fast reaction between H and O atoms was demonstrated to be useful for the O-trapping in the case of pure CO_2 conversion, thus providing a solution for the separation of the CO_2 splitting products [120], but in the present case, it is clearly the limiting factor for the formation of oxygenated hydrocarbons.
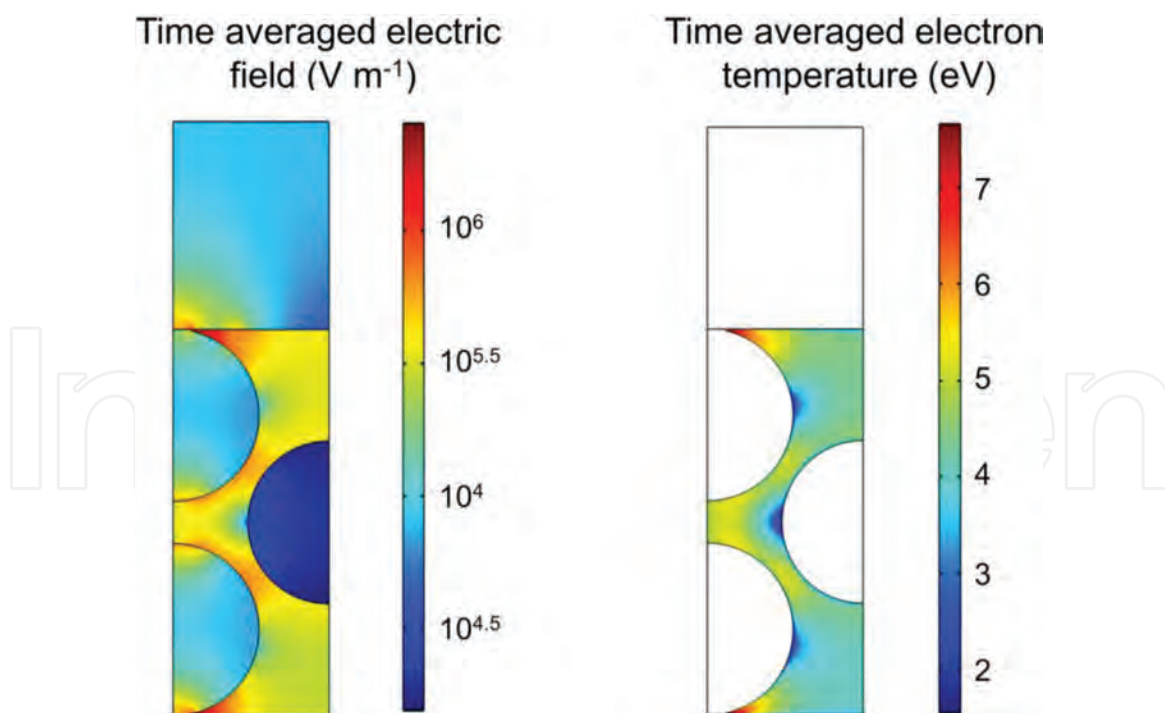
4.1.5 CO_2/N_2 mixture

Real industrial gas flows typically do not contain pure CO_2 but also other gases and impurities. In most cases, N_2 is the most important component. It is thus also important to study the effect of N_2 on the CO_2 conversion and energy efficiency, as well as which products are formed, that is, useful products or harmful NO_x compounds. Hence, we developed some models for a CO_2/N_2 mixture, both for a MW plasma [76] and a DBD [77]. Both models predict that N_2 has a beneficial effect on the CO_2 splitting, but the mechanism is completely different. In a DBD, the electronically excited metastable $N_2(A^3\Sigma_u^+)$ molecules give rise to the enhanced CO_2 splitting [77], while in a MW plasma, the N_2 vibrational levels help to populate the CO_2 vibrational levels, by VV relaxation, and this causes the enhanced CO_2 splitting [76]. It should be mentioned, however, that in spite of the higher absolute CO_2 conversion upon addition of N_2, the effective or overall CO_2 conversion will drop in both cases, because of the lower absolute fraction of CO_2 in the gas mixture. The effect is minor up to about 60% N_2 but more pronounced for higher N_2 fractions. As the effective CO_2 conversion determines the overall energy efficiency of the process, the latter also drops upon addition of more N_2, as some of the energy is used for ionization, excitation, and dissociation of the N_2 molecules.

Both the modeling and experiments also reveal that several NO_x compounds are produced in a CO_2/N_2 plasma, especially NO, NO_2, N_2O, and N_2O_5, as was discussed in detail in [77]. A detailed chemical kinetic analysis reveals how the NO_x compounds are formed and thus also how this formation can be reduced. As illustrated in **Figure 7**, N_2 is excited to a metastable state $N_2(A^3\Sigma_u^+)$, as well as dissociated into N atoms, by electron impact reactions. The $N_2(A^3\Sigma_u^+)$ molecules react with O atoms into NO or with O_2 into N_2O. The N atoms react with both O and O_3 into NO. NO can be converted into NO_2 upon reaction with O, but the opposite reaction, upon collision with either O or N atoms, occurs as well, making NO_2 the main source of NO production and vice versa (see **Figure 7**).

Furthermore, the N atoms are trapped in two reaction loops, that is, between NO, NO_2, and N_2O_3 and between NO_2, NO_3, and N_2O_5. The only way to escape from these loops is by the reaction of NO_2 to N_2O (which can react back to N_2 and N upon collision with $N_2(A^3\Sigma_u^+)$ and N_2^+) or by the reaction of NO with either N atoms or $N_2(a'^1\Sigma_u^-)$ molecules, forming again N atoms or N_2 molecules (see **Figure 7**).

Figure 7.
Dominant reaction pathways leading to NO_x formation in a CO_2/N_2 DBD plasma, as obtained from the model in [77]. See details in the text. The thickness of the arrow lines corresponds to the time-integrated reaction rates, indicating the importance of the reactions. Adopted from [77] with permission.

Figure 7 shows that, in order to avoid the formation of NO_x compounds, we should prevent the reaction between the reactive N-species (i.e., $N_2(A^3\Sigma_u^+)$ and N) and the O species (O, O_2, or O_3). Reducing the concentrations of reactive N-species in the plasma is not straightforward, so we think that a more viable option to avoid NO_x formation is to remove the O atoms from the plasma, by means of O-scavengers, or separation membranes or a catalytic system.

4.2 2D or 3D fluid modeling

While 0D chemical kinetic models are most suitable to elucidate the underlying chemical reaction pathways, they cannot describe detailed effects of reactor design. For this purpose, fluid modeling is more appropriate. We will show here how 2D or 3D fluid models can help to obtain a better insight in the basic characteristics of plasma reactors, using two examples of our group PLASMANT, which are of great interest for the application of CO_2 conversion, that is, packed bed DBD reactors and reverse vortex flow GA reactors.

4.2.1 Packed bed DBD reactors

Packed bed DBD reactors are known to enhance the electric field and thus also the electron temperature, at the contact points between the packing pellets or beads, due to polarization of this dielectric packing. This is illustrated in **Figure 8**, showing the time-averaged electric field and electron temperature distributions in a 2D representation of a packed bed DBD reactor, for a peak-to-peak voltage of 4 kV and a frequency of 23.5 kHz. These results are obtained from a so-called "channel of voids" model, where the packing beads are not in direct contact, but allow the gas flowing through the packing. This is done to allow a 2D model representing a real 3D geometry (see details in [94]). In spite of the fact that there is no real contact between the beads, the local electric field enhancement in between the beads, due to their polarization, is still visible, although it must be mentioned that the effect is
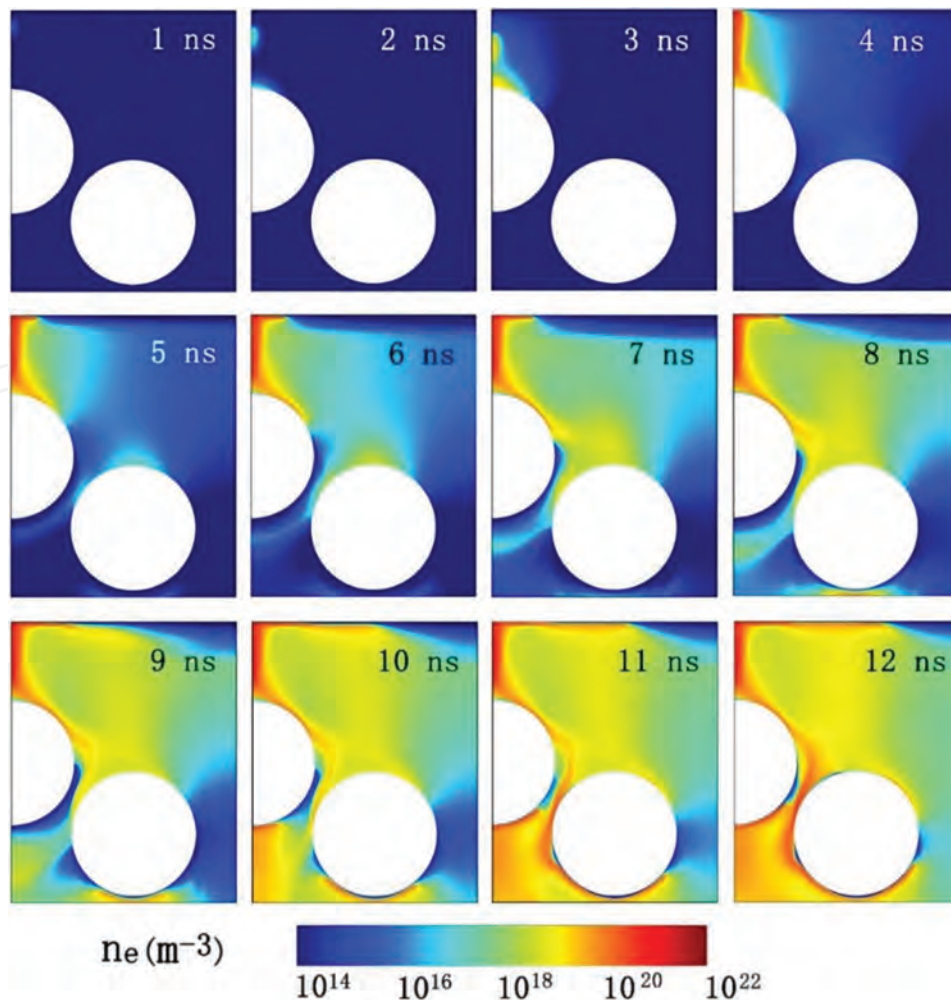
Figure 8.
Calculated time-averaged 2D profiles of the electric field and electron temperature in a packed bed DBD reactor, at a peak-to-peak voltage of 4 kV and a frequency of 23.5 kHz, as obtained from the model in [94]. Adopted from [94] with permission.

more pronounced in a so-called "contact point" model (see [94]). This enhanced electric field gives rise to more electron heating and thus to a higher electron temperature in between the beads (see right panel of **Figure 8**). At this relatively low applied voltage of 4 kV, the plasma is initiated at the contact points and remains in this region, reflecting the properties of a Townsend discharge, while at higher applied voltage, for example, 7.5 kV (peak-to-peak), the discharge will spread out more into the bulk of the reactor, from one void space to the other, ultimately covering the whole gas gap [94]. Such behavior was also reported from experiments. Indeed, by means of an intensified charge-coupled device (ICCD) camera [121, 122], Kim and coworkers also observed that at low applied potential, the discharge stays local at the contact points, while at higher potential, it spreads across the surface of the packing material, and similar observations were also made by Tu et al. [123].

Although the above model was developed for helium, we expect a similar behavior in a CO_2 plasma. The higher electron temperature will give rise to more electron impact ionization, excitation, and dissociation of the CO_2 molecules, for the same applied power, and this can explain why a packed bed DBD gives a higher CO_2 conversion and energy efficiency than an empty reactor.

We also developed a model for a packed bed DBD reactor in dry air, to study the propagation of a plasma streamer [97], as illustrated in **Figures 9** and **10**. Our calculations reveal that the plasma formation in a packed bed DBD reactor in dry air may exhibit three types of discharge behavior, that is, positive restrikes; filamentary microdischarges, also localized between the packing beads; and surface ionization waves, in agreement with the model by Kruszelnicki et al. [93]. Positive restrikes between the dielectrics result in the formation of filamentary microdischarges. Surface charging creates electric field components parallel to the dielectric surface and leads to the formation of surface ionization waves. At a low dielectric constant of the packing (ε_r = 5), plasma ignition between the beads occurs
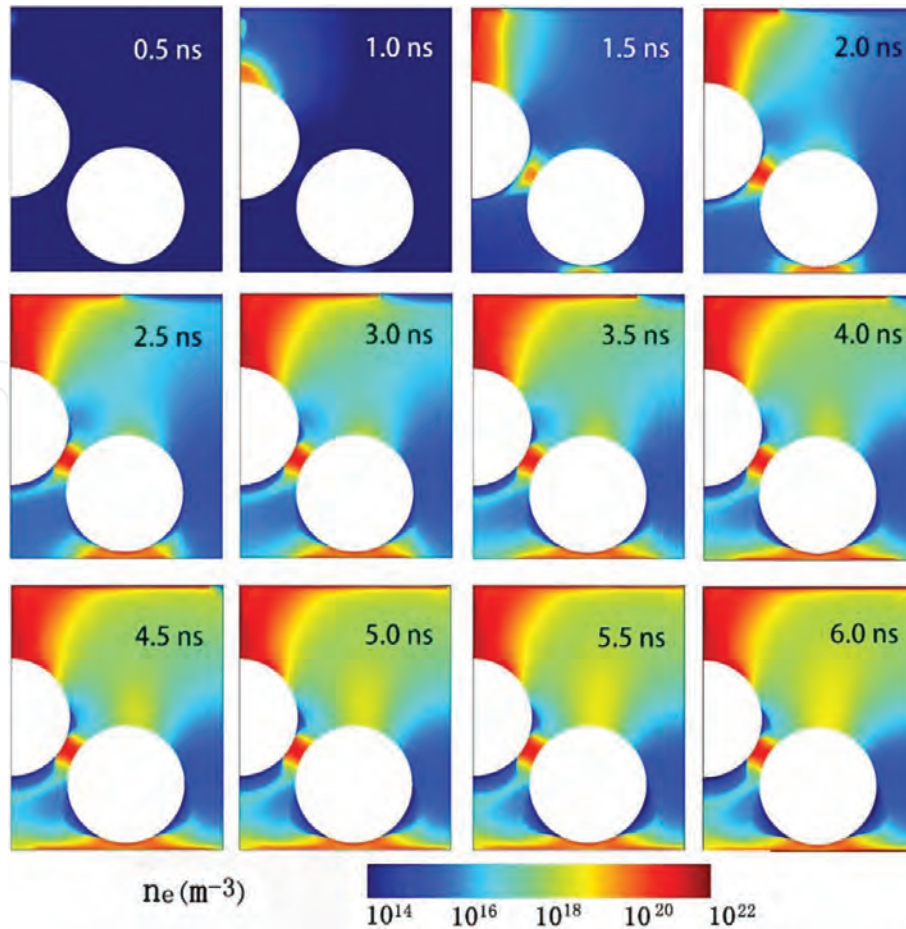
Figure 9.
Calculated electron number density distribution as a function of time, for a packed bed DBD reactor in dry air, with packing beads of ε_r = 5. Adopted from [97] with permission.

directly in the mode of surface discharges (or surface ionization waves), which can connect with the surface of the adjacent bead; see **Figure 9**. On the other hand, at high dielectric constants (ε_r = 1000), no surface streamer jumping toward the adjacent bead surface is observed, and spatially limited filamentary microdischarges, so-called local discharges, are generated between the beads; see **Figure 10**. For intermediate dielectric constants, a mixed mode of surface discharges and local discharges exists [97]. Good qualitative agreement with experiments was obtained, as detailed in [97].

The positive restrikes, local discharges, and surface discharges all give rise to the production of reactive species, because they exhibit an enhanced electric field and thus they create a burst of energetic electrons, which produce reactive species by electron impact dissociation. Packed bed reactors are often used for plasma catalysis, where packing beads with different dielectric constants can act as supports for the catalytic materials. Therefore, this study is important to gain a better insight on how different packing materials can influence the performance of packed bed DBD reactors for plasma catalysis. As our results indicate that a higher dielectric constant constrains the discharge to the contact points of the beads, this may limit the catalyst activation due to the limited catalyst surface area in contact with the discharge, and thus it may have implications for the efficiency of plasma catalytic CO$_2$ conversion. Indeed, the best results are not always reached for the highest dielectric constant [9, 10].

Figure 10.
Calculated electron number density distribution as a function of time, for a packed bed DBD reactor in dry air, with packing beads of ε_r = 1000. Adopted from [97] with permission.

4.2.2 Gliding arc plasmatron (GAP)

Figure 11 illustrates a typical 3D gas flow pattern (a), as well as the calculated electron density profile (b), in a reverse vortex flow (RVF) GA plasma reactor, also called gliding arc plasmatron (GAP), operating in argon. The stream line plot clearly
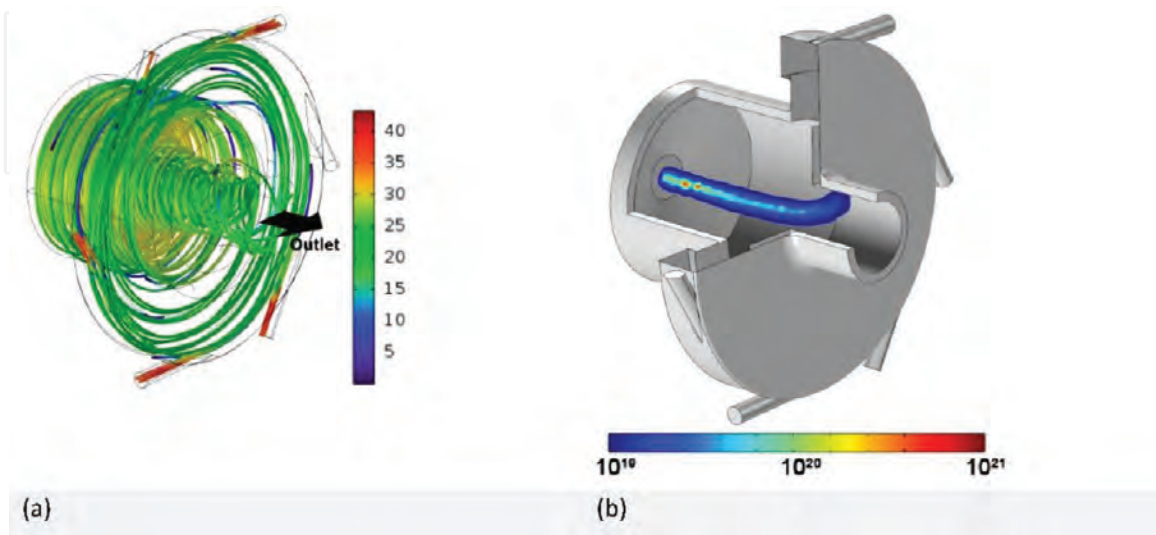
Figure 11.
Calculated steady-state gas flow stream lines (a) and electron density at a time of 5.3 ms, when the arc is stabilized in the center (b), for a reverse vortex flow GA plasma reactor at an arc current of 240 mA, as obtained from the model in [87].

depicts the formation of a reverse vortex flow. The gas is forced into a tangential motion due to the tangential inlets and travels in this way, close to the sidewalls, toward the closed cathode side at the end (= back of **Figure 11(a)**) with a velocity around 30–40 m/s. After it has reached the closed cathode end, it moves in the opposite direction, in a smaller inner (reverse) vortex toward the outlet, with much lower velocity, and it exits the reactor with a velocity around 20 m/s (see also the color scale in **Figure 11(a)**).

The arc plasma reacts to this gas flow pattern, in the sense that when the gas stream is forced to the center, the arc channel will also move to the center (due to convection), and it will stay in this position as long as the gas keeps it stabilized. Hence, the arc plasma is effectively stabilized in the center, as illustrated in **Figure 11(b)**. Furthermore, as the mass transfer is directed toward the center, the walls are thermally insulated from the hot plasma arc column. The fact that no heat is lost to the reactor walls or other parts of the reactor means that more power can be consumed by the discharge, that is, the plasma generation is more effective. Furthermore, keeping the walls insulated (cold) is also beneficial for the reactor materials itself. The calculated plasma density, for an arc current of 240 mA, is around 10^{20} m^{-3}, which is a typical value for GA plasmas at atmospheric pressure.

It should be noted that the results of **Figure 11** are for an argon plasma, but we also developed a similar model for a CO$_2$ plasma, but this was only possible in 2D, because of computation time [87]. However, in the same paper, we also "downgraded" the 3D argon model into 2D, and a comparison between both indicated that the difference between the 3D and 2D argon models was limited. Therefore, the 2D CO$_2$ model provides data with reasonable accuracy. We calculated a typical plasma density of 4×10^{19} m^{-3} in the arc center, which is about one order of magnitude lower than in argon (4×10^{20} m^{-3}), due to other chemical processes, not all leading to ionization.

We can conclude from **Figure 11** that the gas, when moving in the inner vortex flow will largely pass through the arc column. This result is very interesting for the application of CO$_2$ conversion, as it shows that the design of this GAP allows more gas to pass through the arc zone than in a classical (diverging electrodes) GA. Nevertheless, our combined simulations and experiments reveal that the fraction of gas that passes through the arc is still somewhat limited, thus limiting the overall CO$_2$ conversion [19, 20]. By means of this type of 3D fluid dynamics modeling, we aim to predict a more optimized design, to further improve the application of CO$_2$ conversion.

5. Conclusion

Plasma-based CO$_2$ conversion is gaining increasing interest, but to improve this application, we need to obtain a better insight in the underlying mechanisms. The latter can be obtained by both plasma chemistry modeling and plasma reactor modeling. This chapter shows some examples of both modeling approaches from our own group, to illustrate what type of information can be obtained from such models and how this modeling can contribute to a better insight, in order to improve this application.

0D chemical reaction kinetic modeling is very suitable for describing the underlying plasma chemical reaction pathways of the conversion process. We have illustrated this for pure CO$_2$ splitting, showing the difference between a DBD and MW/GA plasma. Indeed, in a DBD, the CO$_2$ conversion is mainly due to electron impact electronic excitation followed by dissociation with the CO$_2$ ground-state molecules,

which requires about 7–10 eV per molecule. This "waste of energy" explains the lower energy efficiency of CO_2 splitting in a DBD. On the other hand, in a MW and GA plasma, vibrational excitation of CO_2 is dominant, and VV relaxation gradually populates the higher vibrational levels (so-called ladder climbing). This is the most energy-efficient way of CO_2 dissociation, as it requires only 5.5 eV per molecule, that is, exactly the C=O bond energy.

We also presented the important reaction pathways in CO_2/CH_4, CH_4/O_2, CO_2/H_2 and CO_2/H_2O mixtures, as well as for the effect of N_2 addition to a CO_2 plasma. In a DBD plasma, the conversion is always initiated by electron impact dissociation, creating radicals that react further into value-added compounds. The main products formed are syngas (CO/H_2), but higher hydrocarbons and oxygenates are also formed in limited amounts. However, the selective production of these targeted compounds is not yet possible, due to the high reactivity of the plasma. Therefore, a catalyst must be inserted in the plasma. Our models reveal that CO_2/CH_4 and CH_4/O_2 mixtures exhibit totally different chemical reactions, resulting in different products. A CO_2/H_2 mixture does not produce many higher hydrocarbons and oxygenates, and the CO_2 conversion is very limited, due to the lack of CH_2 (and CH_3) radical formation. Indeed, the CH_2 radicals are the main collision partners of CO_2 in the CO_2/CH_4 mixture. Furthermore, adding H_2O to a CO_2 DBD plasma yields a drop in CO_2 conversion, and also the H_2O conversion is limited, and virtually no oxygenated hydrocarbons are formed, which could also be explained from the chemical reaction paths. The insights obtained by the model might be useful to provide possible solutions. The last example of 0D chemical kinetic modeling was given for a CO_2/N_2 plasma, where it was shown that also NO_x compounds are produced, which might give several environmental problems. Again, the model can explain their formation, which is useful to provide possible solutions on how to avoid this NO_x formation.

Although 0D models can give useful information on the plasma chemistry, they cannot really account for details in the plasma reactor configuration and thus predict how modifications to the reactor design might lead to improved CO_2 conversion. For this purpose, 2D or 3D fluid models of specific reactor designs are needed. Developing such fluid models for a detailed plasma chemistry, however, leads to excessive calculation times. Therefore, these models are up to now mainly developed for simpler chemistry, in argon or helium. We have shown here examples for a packed bed DBD reactor and a GAP. These models allow to elucidate why certain reactor designs give beneficial results and to pinpoint the limitations and finally how improvements in the reactor designs might yield a better CO_2 conversion and energy efficiency.

In the future work, we intend to implement the more complex CO_2 chemistry (either pure or mixed with other gases) in such fluid models, to obtain a more comprehensive picture of CO_2 conversion in a real plasma reactor geometry. As this is quite challenging in terms of computation time, reduced chemistry sets must be developed for CO_2 and its gas mixtures. When modeling CO_2 conversion in a MW or GA plasma, the vibrational kinetics must be accounted for. To avoid the need of describing all individual levels, we have developed a level-lumping strategy [39], which enables to group the vibrational levels of the asymmetric stretch mode of CO_2 into a number of groups. This reduces the calculation time, so that it can be implemented in 2D models [86]. We believe that a combination of 0D chemical kinetic models (to obtain detailed insight in the entire plasma chemistry and to develop reduced chemistry sets, identifying the main species and chemical reactions) and 2D/3D fluid models (for a detailed understanding of the reactor design) is the most promising approach to make further progress in this field.

Acknowledgements

Author details

Annemie Bogaerts[1*], Ramses Snoeckx[1,2], Georgi Trenchev[1] and Weizong Wang[1,3]

1 Department of Chemistry, Research Group PLASMANT, University of Antwerp, Belgium

2 Clean Combustion Research Center (CCRC), Physical Science and Engineering Division (PSE), King Abdullah University of Science and Technology (KAUST), Saudi Arabia

3 School of Astronautics, Beihang University, Beijing, P.R. China

*Address all correspondence to: annemie.bogaerts@uantwerpen.be

IntechOpen

References

[1] Snoeckx R, Bogaerts A. Plasma technology - a novel solution for CO_2 conversion? Chemical Society Reviews. 2017;**46**:5805-5863

[2] Paulussen S, Verheyde B, Tu X, De Bie C, Martens T, Petrovic D, et al. Conversion of carbon dioxide to value-added chemicals in atmospheric pressure dielectric barrier discharges. Plasma Sources Science and Technology. 2010;**19**:034015

[3] Tu X, Gallon HJ, Twigg MV, Gorry PA, Whitehead JC. Dry reforming of methane over a Ni/Al_2O_3 catalyst in a coaxial dielectric barrier discharge reactor. Journal of Physics D: Applied Physics. 2011;**44**:274007

[4] Gómez-Ramírez A, Rico VJ, Cotrino J, González-Elipe AR, Lambert RM. Low temperature production of formaldehyde from carbon dioxide and ethane by plasma-assisted catalysis in a ferroelectrically moderated dielectric barrier discharge reactor. ACS Catalysis. 2014;**4**:402-408

[5] Scapinello M, Martini LM, Tosi P. CO_2 hydrogenation by CH_4 in a dielectric barrier discharge: Catalytic effect of Ni and Cu. Plasma Processes and Polymers. 2014;**11**:624-628

[6] Ozkan A, Dufour T, Arnoult G, De Keyzer P, Bogaerts A, Reniers F. CO_2-CH_4 conversion and syngas formation at atmospheric pressure using a multi-electrode dielectric barrier discharge. Journal of CO_2 Utilization. 2015;**9**:74-81

[7] Aerts R, Somers W, Bogaerts A. Carbon dioxide splitting in a dielectric barrier discharge plasma: A combined experimental and computational study. ChemSusChem. 2015;**8**:702-716

[8] Van Laer K, Bogaerts A. Improving the conversion and energy efficiency of carbon dioxide splitting in a zirconia-packed dielectric barrier discharge reactor. Energy Technology. 2015;**3**: 1038-1044

[9] Michielsen I, Uytdenhouwen Y, Pype J, Michielsen B, Mertens J, Reniers F, et al. CO_2 dissociation in a packed bed DBD reactor: First steps towards a better understanding of plasma catalysis. Chemical Engineering Journal. 2017; **326**:477-488

[10] Uytdenhouwen Y, Van Alphen S, Michielsen I, Meynen V, Cool P, Bogaerts A. A packed-bed DBD micro plasma reactor for CO_2 dissociation: Does size matter? Chemical Engineering Journal. 2018;**348**:557-568

[11] Silva T, Britun N, Godfroid T, Snyders R. Optical characterization of a microwave pulsed discharge used for dissociation of CO_2. Plasma Sources Science and Technology. 2014;**23**: 025009

[12] Bongers W, Bouwmeester H, Wolf B, Peeters F, Welzel S, van den Bekerom D, et al. Plasma-driven dissociation of CO_2 for fuel synthesis. Plasma Processes and Polymers. 2017;**16**:1600126

[13] van Rooij GJ, van den Bekerom DCM, den Harder N, Minea T, Berden G, Bongers WA, et al. Taming microwave plasma to beat thermodynamics in CO_2 dissociation. Faraday Discussions. 2015;**183**:233-248

[14] Scapinello M, Martini LM, Dilecce G, Tosi P. Conversion of CH_4/CO_2 by a nanosecond repetitively pulsed discharge. Journal of Physics D: Applied Physics. 2016;**49**:075602

[15] Zhu B, Li XS, Liu JL, Zhu X, Zhu AM. Kinetics study on carbon dioxide reforming of methane in kilohertz

spark-discharge plasma. Chemical Engineering Journal. 2015;**264**:445-452

[16] Nunnally T, Gutsol K, Rabinovich A, Fridman A, Gutsol A, Kemoun A. Dissociation of CO$_2$ in a low current gliding arc plasmatron. Journal of Physics D: Applied Physics. 2011;**44**: 274009

[17] Tu X, Whitehead JC. Plasma dry reforming of methane in an atmospheric pressure AC gliding arc discharge: Co-generation of syngas and carbon nanomaterials. International Journal of Hydrogen Energy. 2014;**39**:9658-9669

[18] Liu JL, Park HW, Chung WJ, Ahn WS, Park DW. Simulated biogas oxidative reforming in AC-pulsed gliding arc discharge. Chemical Engineering Journal. 2016;**285**:243-251

[19] Ramakers M, Trenchev G, Heijkers S, Wang W, Bogaerts A. Gliding arc plasmatron: Providing an alternative method for carbon dioxide conversion. ChemSusChem. 2017;**10**:2642-2652

[20] Cleiren E, Heijkers S, Ramakers M, Bogaerts A. Dry reforming of methane in a gliding arc plasmatron: Towards a better understanding of the plasma chemistry. ChemSusChem. 2017;**10**: 4025-4036

[21] Neyts EC, Ostrikov K, Sunkara MK, Bogaerts A. Plasma catalysis: Synergistic effects at the nanoscale. Chemical Reviews. 2015;**115**:13408-13446

[22] Hokazono H, Fujimoto H. Theoretical analysis of the CO$_2$ molecule decomposition and contaminants yield in transversely excited atmospheric CO$_2$ laser discharge. Journal of Applied Physics. 1987;**62**:1585-1594

[23] Cenian A, Chernukho A, Borodin V, Sliwinski G. Modeling of plasma-chemical reactions in gas mixture of CO$_2$ lasers I. gas decomposition in pure

CO$_2$ glow discharge. Contributions to Plasma Physics. 1994;**34**:25-37

[24] Cenian A, Chernukho A, Borodin V. Modeling of plasma-chemical reactions in gas mixture of CO$_2$ lasers. II. Theoretical model and its verification. Contributions to Plasma Physics. 1995; **35**:273-296

[25] Gordiets BF, Osipov AI, Stupochenko EV, Shelepin LA. Vibrational relaxation in gases and molecular lasers. Soviet Physics Uspekhi. 1973;**15**:759-785

[26] Kustova E, Nagnibeda E. On a correct description of a multi-temperature dissociating CO$_2$ flow. Chemical Physics. 2006;**321**:293-310

[27] Rusanov VD, Fridman AA, Sholin GV. The physics of a chemically active plasma with nonequilibrium vibrational excitation of molecules. Soviet Physics Uspekhi. 1981;**24**:447-474

[28] Aerts R, Martens T, Bogaerts A. Influence of vibrational states on CO$_2$ splitting by dielectric barrier discharges. Journal of Physical Chemistry C. 2012; **116**:23257-23273

[29] Kozák T, Bogaerts A. Splitting of CO$_2$ by vibrational excitation in non-equilibrium plasmas: A reaction kinetics model. Plasma Sources Science and Technology. 2014;**23**:045004

[30] Kozák T, Bogaerts A. Evaluation of the energy efficiency of CO$_2$ conversion in microwave discharges using a reaction kinetics model. Plasma Sources Science and Technology. 2015;**24**: 015024

[31] Ponduri S, Becker MM, Welzel S, van de Sanden MCM, Loffhagen D, Engeln R. Fluid modelling of CO$_2$ dissociation in a dielectric barrier discharge. Journal of Applied Physics. 2016;**119**:093301

[32] Pietanza LD, Colonna G, D'Ammando G, Laricchiuta A, Capitelli M. Vibrational excitation and dissociation mechanisms of CO_2 under non-equilibrium discharge and post-discharge conditions. Plasma Sources Science and Technology. 2015;**24**: 042002

[33] Pietanza LD, Colonna G, D'Ammando G, Laricchiuta A, Capitelli M. Non equilibrium vibrational assisted dissociation and ionization mechanisms in cold CO_2 plasmas. Chemical Physics. 2016;**468**:44-52

[34] Pietanza LD, Colonna G, D'Ammando G, Laricchiuta A, Capitelli M. Electron energy distribution functions and fractional power transfer in "cold" and excited CO_2 discharge and post discharge conditions. Physics of Plasmas. 2016;**23**:013515

[35] Pietanza LD, Colonna G, Laporta V, Celiberto R, D'Ammando G, Laricchiuta A, et al. Influence of electron molecule resonant vibrational collisions over the symmetric mode and direct excitation-dissociation cross sections of CO_2 on the electron energy distribution function and dissociation mechanisms in cold pure CO_2 plasmas. The Journal of Physical Chemistry. A. 2016;**120**: 2614-2628

[36] Pietanza LD, Colonna G, D'Ammando G, Capitelli M. Time-dependent coupling of electron energy distribution function, vibrational kinetics of the asymmetric mode of CO_2 and dissociation, ionization and electronic excitation kinetics under discharge and post-discharge conditions. Plasma Physics and Controlled Fusion. 2016;**59**:014035

[37] Koelman P, Heijkers S, Tadayon Mousavi S, Graef W, Mihailova D, Kozák T, et al. A comprehensive chemical model for the splitting of CO_2 in non-equilibrium plasmas. Plasma Processes and Polymers. 2017;**14**: 1600155

[38] Chen JL, Wang HX, Sun SR. Analysis of dissociation mechanism of CO_2 in a micro-hollow cathode discharge. Chinese Physics Letters. 2016;**33**:108201

[39] Berthelot A, Bogaerts A. Modeling of plasma-based CO_2 conversion: Lumping of the vibrational levels. Plasma Sources Science and Technology. 2016;**25**:045022

[40] de la Fuenta JF, Moreno SH, Stankiewicz AI, Stefanidis GD. A new methodology for the reduction of vibrational kinetics in non-equilibrium microwave plasma: Application to CO_2 dissociation. Reaction Chemistry & Engineering. 2016;**1**:540-554

[41] Moss M, Yanallah K, Allen R, Pontiga F. An investigation of CO_2 splitting using nanosecond pulsed corona discharge: Effect of argon addition on CO_2 conversion and energy efficiency. Plasma Sources Science and Technology. 2017;**26**:035009

[42] Berthelot A, Bogaerts A. Modeling of CO_2 splitting in a microwave plasma: How to improve the conversion and energy efficiency. Journal of Physical Chemistry C. 2017;**121**:8236-8251

[43] Berthelot A, Bogaerts A. Pinpointing energy losses in CO_2 plasmas - effect on CO_2 conversion. Journal of CO_2 Utilization. 2018;**24**: 479-499

[44] Wang W, Berthelot A, Kolev S, Tu X, Bogaerts A. CO_2 conversion in a gliding arc plasma: 1D cylindrical discharge model. Plasma Sources Science and Technology. 2016;**25**: 065012

[45] Sun SR, Wang HX, Mei DH, Tu X, Bogaerts A. CO_2 conversion in a gliding arc plasma: Performance improvement

based on chemical reaction modeling. Journal of CO$_2$ Utilization. 2017;**17**: 220-234

[46] Berthelot A, Bogaerts A. Modeling of CO$_2$ plasma: Effect of uncertainties in the plasma chemistry. Plasma Sources Science and Technology. 2017;**26**: 115002

[47] Heijkers S, Bogaerts A. CO$_2$ conversion in a gliding arc plasmatron: Elucidating the chemistry through kinetic modeling. Journal of Physical Chemistry C. 2017;**121**:22644-22655

[48] Bogaerts A, Wang W, Berthelot A, Guerra V. Modeling plasma-based CO$_2$ conversion: Crucial role of the dissociation cross section. Plasma Sources Science and Technology. 2016; **25**:055016

[49] Indarto A, Choi JW, Lee H, Song HK. Kinetic modeling of plasma methane conversion using gliding arc. Journal of Natural Gas Chemistry. 2005; **14**:13-21

[50] Indarto A, Coowanitwong N, Choi JW, Lee H, Song HK. Kinetic modeling of plasma methane conversion in a dielectric barrier discharge. Fuel Processing Technology. 2008;**89**: 214-219

[51] Yang Y. Direct non-oxidative methane conversion by non-thermal plasma: Modeling study. Plasma Chemistry and Plasma Processing. 2003; **23**:327

[52] De Bie C, Verheyde B, Martens T, van Dijk J, Paulussen S, Bogaerts A. Fluid modelling of the conversion of methane into higher hydrocarbons in an atmospheric pressure dielectric barrier discharge. Plasma Processes and Polymers. 2011;**8**:1033-1058

[53] Luche J, Aubry O, Khacef A, Cormier JM. Syngas production from methane oxidation using a non-thermal plasma: Experiments and kinetic modeling. Chemical Engineering Journal. 2009;**149**:35-41

[54] Zhou LM, Xue B, Kogelschatz U, Eliasson B. Nonequilibrium plasma reforming of greenhouse gases to synthesis gas. Energy & Fuels. 1998;**12**: 1191-1199

[55] Machrafi H, Cavadias S, Amouroux J. CO$_2$ valorization by means of dielectric barrier discharge. Journal of Physics: Conference Series. 2011;**275**: 012016

[56] Goujard V, Tatibouet JM, Batiot-Dupeyrat C. Carbon dioxide reforming of methane using a dielectric barrier discharge reactor: Effect of helium dilution and kinetic model. Plasma Chemistry and Plasma Processing. 2011; **31**:315-325

[57] Wang JG, Liu CJ, Eliasson B. Density functional theory study of synthesis of oxygenates and higher hydrocarbons from methane and carbon dioxide using cold plasmas. Energy & Fuels. 2004;**18**: 148-153

[58] Istadi I, Amin NAS. Modelling and optimization of catalytic–dielectric barrier discharge plasma reactor for methane and carbon dioxide conversion using hybrid artificial neural network—Genetic algorithm technique. Chemical Engineering Science. 2007;**62**:6568-6581

[59] Kraus M, Egli W, Haffner K, Eliasson B, Kogelschatz U, Wokaun A. Investigation of mechanistic aspects of the catalytic CO$_2$ reforming of methane in a dielectric-barrier discharge using optical emission spectroscopy and kinetic modeling. Physical Chemistry Chemical Physics. 2002;**4**:668-675

[60] Liu CJ, Li Y, Zhang YP, Wang Y, Zou J, Eliasson B, et al. Production of acetic acid directly from methane and carbon dioxide using dielectric-barrier

discharges. Chemistry Letters. 2001;**30**: 1304-1305

[61] De Bie C, Martens T, van Dijk J, Paulussen S, Verheyde B, Bogaerts A. Dielectric barrier discharges used for the conversion of greenhouse gases: Modeling the plasma chemistry by fluid simulations. Plasma Sources Science and Technology. 2011;**20**:024008

[62] Snoeckx R, Aerts R, Tu X, Bogaerts A. Plasma-based dry reforming: A computational study ranging from the nanoseconds to seconds time scale. Journal of Physical Chemistry C. 2013;**117**:4957-4970

[63] Snoeckx R, Zeng YX, Tu X, Bogaerts A. Plasma-based dry reforming: Improving the conversion and energy efficiency in a dielectric barrier discharge. RSC Advances. 2015;**5**: 29799-29808

[64] Janeco A, Pinhão NR, Guerra V. Electron kinetics in He/CH_4/CO_2 mixtures used for methane conversion. Journal of Physical Chemistry C. 2015; **119**:109-120

[65] Wang W, Berthelot A, Zhang QZ, Bogaerts A. Modelling of plasma-based dry reforming: How do uncertainties in the input data affect the calculation results? Journal of Physics D: Applied Physics. 2018;**51**:204003

[66] De Bie C, van Dijk J, Bogaerts A. The dominant pathways for the conversion of methane into oxygenates and syngas in an atmospheric pressure dielectric barrier discharge. Journal of Physical Chemistry C. 2015;**119**: 22331-22350

[67] Zhou LM, Xue B, Kogelschatz U, Eliasson B. Partial oxidation of methane to methanol with oxygen or air in a nonequilibrium discharge plasma. Plasma Chemistry and Plasma Processing. 1998;**18**:375-393

[68] Nair SA, Nozaki T, Okazaki K. Methane oxidative conversion pathways in a dielectric barrier discharge reactor —Investigation of gas phase mechanism. Chemical Engineering Journal. 2007;**132**:85-95

[69] Goujard V, Nozaki T, Yuzawa S, Ağiral A, Okazaki K. Plasma-assisted partial oxidation of methane at low temperatures: Numerical analysis of gas-phase chemical mechanism. Journal of Physics D: Applied Physics. 2011;**44**: 274011

[70] Agiral A, Nozaki T, Nakase M, Yuzawa S, Okazaki K, Gardeniers JGE. Chemical Engineering Journal. 2011;**167**: 560

[71] Zhou J, Xu Y, Zhou X, Gong J, Yin Y, Zheng H, et al. Direct oxidation of methane to hydrogen peroxide and organic oxygenates in a double dielectric plasma reactor. ChemSusChem. 2011;**4**: 1095-1098

[72] Matin NS, Whitehead JC. A chemical model for the atmospheric pressure plasma reforming of methane with oxygen. In: 28th ICPIG, 15–20 July 2007; Prague, Czech Republic. 2007. p. 983

[73] Snoeckx R, Ozkan O, Reniers F, Bogaerts A. The quest for value-added products from carbon dioxide and water in a dielectric barrier discharge: A chemical kinetics study. ChemSusChem. 2017;**10**:409-424

[74] Eliasson B, Kogelschatz U, Xue B, Zhou LM. Hydrogenation of carbon dioxide to methanol with a discharge-activated catalyst. Industrial and Engineering Chemistry Research. 1998; **37**:3350-3357

[75] De Bie C, van Dijk J, Bogaerts A. CO_2 hydrogenation in a dielectric barrier discharge plasma revealed. Journal of Physical Chemistry C. 2016; **120**:25210-25224

[76] Heijkers S, Snoeckx R, Kozák T, Silva T, Godfroid T, Britun N, et al. CO_2 conversion in a microwave plasma reactor in the presence of N_2: Elucidating the role of vibrational levels. Journal of Physical Chemistry C. 2015; **119**:12815-12828

[77] Snoeckx R, Heijkers S, Van Wesenbeeck K, Lenaerts S, Bogaerts A. CO_2 conversion in a dielectric barrier discharge plasma: N_2 in the mix as a helping hand or problematic impurity? Energy & Environmental Science. 2016; **9**:999-1011

[78] Legrand J, Diamy A, Hrach R, Hrachova V. Kinetics of reactions in CH_4/N_2 afterglow plasma. Vacuum. 1997;**48**:671-675

[79] Majumdar A, Behnke JF, Hippler R, Matyash K, Schneider R. Chemical reaction studies in CH_4/Ar and CH_4/N_2 gas mixtures of a dielectric barrier discharge. The Journal of Physical Chemistry. A. 2005;**109**:9371-9377

[80] Pintassiglio CD, Jaoul C, Loureiro J, Belmonte T, Czerwiec T. Kinetic modelling of a N_2 flowing microwave discharge with CH_4 addition in the post-discharge for nitrocarburizing treatments. Journal of Physics D: Applied Physics. 2007;**40**:3620-3632

[81] Jauberteau JL, Jauberteau I, Cinelli MJ, Aubreton J. Reactivity of methane in a nitrogen discharge afterglow. New Journal of Physics. 2002;**4**:39

[82] Savinov SY, Lee H, Keun H, Na B. The effect of vibrational excitation of molecules on plasmachemical reactions involving methane and nitrogen. Plasma Chemistry and Plasma Processing. 2003; **23**:159-173

[83] Snoeckx R, Setareh M, Aerts R, Simon P, Maghari A, Bogaerts A. Influence of N_2 concentration in a CH_4/N_2 dielectric barrier discharge used for CH_4 conversion into H_2. International Journal of Hydrogen Energy. 2013;**38**: 16098-16120

[84] Bogaerts A, De Bie C, Snoeckx R, Kozák T. Plasma based CO_2 and CH_4 conversion: A modeling perspective. Plasma Processes and Polymers. 2017; **14**:e1600070

[85] Wang W, Snoeckx R, Zhang X, Cha MS, Bogaerts A. Modeling plasma-based CO_2 and CH_4 conversion in mixtures with N_2, O_2 and H_2O: The bigger plasma chemistry picture. Journal of Physical Chemistry C. 2018;**122**:8704-8723

[86] Wang W, Mei D, Tu X, Bogaerts A. Gliding arc plasma for CO_2 conversion: Better insights by a combined experimental and modelling approach. Chemical Engineering Journal. 2017; **330**:11-25

[87] Trenchev G, Kolev S, Wang W, Ramakers M, Bogaerts A. CO_2 conversion in a gliding arc plasmatron: Multidimensional modeling for improved efficiency. Journal of Physical Chemistry C. 2017;**121**:24470-24479

[88] Chang JS, Kostov KG, Urashima K, Yamamoto T, Okayasu Y, Kato T, et al. Removal of NF_3 from semiconductor-process flue gases by tandem packed-bed plasma and adsorbent hybrid systems. IEEE Transactions on Industry Applications. 2000;**36**:1251-1259

[89] Takaki K, Chang JS, Kostov KG. Atmospheric pressure of nitrogen plasmas in a ferroelectric packed bed barrier discharge reactor. Part I. modeling. IEEE Transactions on Dielectrics and Electrical Insulation. 2004;**11**:481-490

[90] Zhang Y, Wang HY, Jiang W, Bogaerts A. Two-dimensional particle-in cell/Monte Carlo simulations of a packed-bed dielectric barrier discharge in air at atmospheric pressure. New Journal of Physics. 2015;**17**:083056

[91] Kang WS, Park JM, Kim Y, Hong SH. Numerical study on influences of barrier arrangements on dielectric barrier discharge characteristics. IEEE Transactions on Plasma Science. 2003; **31**:504-510

[92] Russ H, Neiger M, Lang JE. Simulation of micro discharges for the optimization of energy requirements for removal of NO_x from exhaust gases. IEEE Transactions on Plasma Science. 1999;**27**:38-39

[93] Kruszelnicki J, Engeling KW, Foster JE, Xiong Z, Kushner MJ. Propagation of negative electrical discharges through 2-dimensional packed bed reactors. Journal of Physics D: Applied Physics. 2017;**50**:025203

[94] Van Laer K, Bogaerts A. Fluid modelling of a packed bed dielectric barrier discharge plasma reactor. Plasma Sources Science and Technology. 2016; **25**:015002

[95] Van Laer K, Bogaerts A. Influence of gap size and dielectric constant of the packing material on the plasma behaviour in a packed bed DBD reactor: A fluid modelling study. Plasma Processes and Polymers. 2017;**14**: e1600129

[96] Van Laer K, Bogaerts A. How bead size and dielectric constant affect the plasma behaviour in a packed bad plasma reactor: A modelling study. Plasma Sources Science and Technology. 2017;**26**:085007

[97] Wang W, Kim HH, Van Laer K, Bogaerts A. Streamer propagation in a packed bed plasma reactor for plasma catalysis applications. Chemical Engineering Journal. 2018;**334**: 2467-2479

[98] Kang WS, Kim HH, Teramoto Y, Ogata A, Lee JY, Kim DW, et al. Surface streamer propagations on an alumina bead: Experimental observation and numerical modeling. Plasma Sources Science and Technology. 2018;**27**: 015018

[99] Georgieva V, Berthelot A, Silva T, Kolev S, Graef W, Britun N, et al. Understanding microwave surface-wave sustained plasmas at intermediate pressure by 2D modeling and experiments. Plasma Processes and Polymers. 2017;**14**:e1600185

[100] Janssen GM. Design of a general plasma simulation model: Fundamental aspects and applications. PhD thesis. Eindhoven University of Technology, the Netherlands; 2000. 186 p

[101] Jimenez-Diaz M, Carbone EAD, van Dijk J, van der Mullen JJAM. A two-dimensional Plasimo multiphysics model for the plasma–electromagnetic interaction in surface wave discharges: The surfatron source. Journal of Physics D: Applied Physics. 2012;**45**:335204

[102] Rahimi S, Jimenez-Diaz M, Hubner S, Kemaneci EH, van der Mullen JJAM, van Dijk J. A two-dimensional modelling study of a coaxial plasma waveguide. Journal of Physics D: Applied Physics. 2014;**47**:125204

[103] Kabouzi Y, Graves DB, Castanos-Martınez E, Moisan M. Modeling of atmospheric-pressure plasma columns sustained by surface waves. Physical Review E. 2007;**75**:016402

[104] Richard F, Cormier JM, Pellerin S, Chapelle J. Physical study of a gliding arc discharge. Journal of Applied Physics. 1996;**79**:2245-2250

[105] Fridman A, Nester S, Kennedy LA, Saveliev A, Mutaf-Yardemci O. Gliding arc gas discharge. Progress in Energy and Combustion Science. 1999;**25**: 211-231

[106] Pellerin S, Richard F, Chapelle J, Cormier JM, Musiol K. Heat string model of bi-dimensional dc Glidarc. Journal of Physics D: Applied Physics. 2000;**33**:2407-2419

[107] Mutaf-Yardimci O, Saveliev AV, Fridman AA, Kennedy LA. Thermal and nonthermal regimes of gliding arc discharge in air flow. Journal of Applied Physics. 2000;**87**:1632-1641

[108] Kuznetsova IV, Kalashnikov NY, Gutsol AF, Fridman AA, Kennedy LA. Effect of "overshooting" in the transitional regimes of the low-current gliding arc discharge. Journal of Applied Physics. 2002;**92**:4231-4237

[109] Pellerin S, Cormier JM, Richard F, Musiol K, Chapelle J. Determination of the electrical parameters of a bi-dimensional d.c. Glidarc. Journal of Physics D: Applied Physics. 1999;**32**: 891-897

[110] Gutsol AF, Gangoli SP. Transverse 2-D gliding arc modeling. IEEE Transactions on Plasma Science. 2017; **45**:555-564

[111] Kolev S, Bogaerts A. A 2D model for a gliding arc discharge. Plasma Sources Science and Technology. 2015; **24**:015025

[112] Kolev S, Bogaerts A. Similarities and differences between gliding glow and gliding arc discharges. Plasma Sources Science and Technology. 2015; **24**:065023

[113] Kolev S, Sun SR, Trenchev G, Wang W, Wang HX, Bogaerts A. Quasi-neutral modeling of gliding arc plasmas. Plasma Processes and Polymers. 2017; **14**:e1600110

[114] Sun SR, Kolev S, Wang HX, Bogaerts A. Coupled gas flow-plasma model for a gliding arc: Investigations of

the back-breakdown phenomenon and its effect on the gliding arc characteristics. Plasma Sources Science and Technology. 2017;**26**:015003

[115] Trenchev G, Kolev S, Bogaerts A. A 3D model of a reverse vortex flow gliding arc reactor. Plasma Sources Science and Technology. 2016;**25**: 035014

[116] Bogaerts A, Berthelot A, Heijkers S, Kolev S, Snoeckx R, Sun S, et al. CO$_2$ conversion by plasma technology: Insights from modeling the plasma chemistry and plasma reactor design. Plasma Sources Science and Technology. 2017;**26**:063001

[117] Fridman A. Plasma Chemistry. Cambridge: Cambridge University Press; 2008. 1022 p

[118] Hagelaar GJM, Pitchford LC. Solving the Boltzmann equation to obtain electron transport coefficients and rate coefficients for fluid models. Plasma Sources Science and Technology. 2005;**14**:722-733

[119] Bogaerts A, Kozák T, Van Laer K, Snoeckx R. Plasma-based conversion of CO$_2$: Current status and future challenges. Faraday Discussions. 2015; **183**:217-232

[120] Aerts R, Snoeckx R, Bogaerts A. In-situ chemical trapping of oxygen in the splitting of carbon dioxide by plasma. Plasma Processes and Polymers. 2014;**11**:985-992

[121] Kim HH, Wang N, Ogata A, Song YH. Propagation of surface streamers on the surface of HSY zeolites-supported silver nanoparticles. IEEE Transactions on Plasma Science. 2011;**39**:2220-2221

[122] Kim HH, Ogata A. Interaction of nonthermal plasma with catalyst for the air pollution control. International

journal of Environmental Science and Technology. 2012;**6**:43-48

[123] Tu X, Gallon HJ, Whitehead JC. Transition behavior of packed-bed dielectric barrier discharge in argon. IEEE Transactions on Plasma Science. 2011;**39**:2172-2173